Original Article

DOI: 10.5582/bst.2026.01202

ATP6L impairs vascular stability in colorectal cancer *via* PDGFB/PDGFRβ signaling

Xiangdong Tian[1,§,*], Dandan Chen[1,2,§], Jiaqi Duo[1,§], Shi Zhang[1], Lisha Qi[1,*]

[1] Tianjin Medical University Cancer Institute and Hospital, National Clinical Research Center for Cancer, Tianjin Key Laboratory of Digestive Cancer, Tianjin's Clinical Research Center for Cancer, State Key Laboratory of Druggability Evaluation and Systematic Translational Medicine, Tianjin, China;
[2] Department of Pathology, Cangzhou People's Hospital, Cangzhou, Hebei, China.

SUMMARY: Vascular instability, characterized by impaired pericyte coverage, is a hallmark of tumor progression. ATP6L is highly expressed in colorectal cancer (CRC) tissues and promotes tumor progression by enhancing the tumor microvasculature; however, its direct impact on vascular stability remains unclear. ATP6L expression, microvascular morphology, and pericyte coverage were analyzed by immunohistochemistry in a cohort of 179 CRC specimens, and the role of ATP6L in vascular stability was further investigated by modulating its expression both *in vitro* and *in vivo*. *In vitro*, MC38 and CT26 cells with ATP6L overexpression or knockdown were co-cultured with mouse vascular smooth muscle cells (MOVAS), and MOVAS proliferation, migration, and apoptosis were evaluated using EdU incorporation, transwell migration, and TUNEL staining assays, respectively. PDGFB secretion and PDGFRβ expression were assessed by ELISA, Western blotting, and immunofluorescence. Along the normal colorectal mucosa–adenoma–adenocarcinoma sequence, ATP6L upregulation was closely associated with progressive vascular instability, characterized by loss of pericyte coverage and increasing vascular morphological heterogeneity. Mechanistically, ATP6L overexpression promoted extracellular acidification, suppressed PDGFB secretion, and subsequently reduced PDGFRβ expression in pericytes, thereby impairing their recruitment and survival. Conversely, ATP6L knockdown attenuated extracellular acidification, restored PDGFB/PDGFRβ signaling, and rescued pericyte proliferation, migration, and survival. These findings identify ATP6L as a key mediator of perivascular dysfunction in CRC and demonstrate that ATP6L-induced extracellular acidification disrupts vascular stability by suppressing the PDGFB/PDGFRβ signaling axis and impairing pericyte function.

Keywords: colorectal cancer, ATP6L, vascular stability, pericytes, PDGFB/PDGFRβ signaling

1. Introduction

Abnormal tumor vasculature, characterized by structural fragility and functional inefficiency, is a critical hallmark of cancer (*1,2*). Beyond the mere formation of new blood vessels (angiogenesis), the stability and maturation of these vessels are essential for efficient perfusion and drug delivery (*3,4*). Conversely, vascular instability—marked by chaotic architecture, high permeability, and poor pericyte coverage (*1,5,6*)—promotes hypoxia, immune evasion, and metastasis. This understanding has shifted the therapeutic focus towards vascular normalization, a strategy aimed at restoring vessel integrity. In this context, pericytes, the mural cells that envelop capillaries, are crucial gatekeepers of vascular stability (*7,8*). Their recruitment, adhesion, and function are tightly regulated, and their depletion is a hallmark of the immature, dysfunctional tumor vasculature (*5,9*).

A principal driver of the hostile tumor microenvironment is extracellular acidosis (*10,11*), predominantly mediated by the vacuolar H+-ATPase (V-ATPase) proton pump (*12*). As a key functional subunit of the V-ATPase complex, ATP6L is commonly upregulated in malignancies (*13*). Through its promotion of extracellular acidification, ATP6L has been firmly implicated in promoting aggressive tumor behaviors, including enhanced invasiveness and acquired chemoresistance, underscoring its multifaceted pro-tumorigenic functions (*14-16*). However, despite the well-recognized role of ATP6L-driven acidosis in remodeling the tumor microenvironment, its direct impact on the tumor vasculature—particularly on pericyte function and vascular stability—remains largely unexplored. Although the acidic niche is known to broadly influence stromal cells (*10,17*), the specific molecular mechanisms by which cancer cell-derived

ATP6L compromises pericyte integrity and disrupts vascular homeostasis in colorectal cancer (CRC) remain to be elucidated.

In this study, we identify ATP6L as a critical driver of perivascular dysfunction in CRC. The normal–adenoma–carcinoma progression in colorectal cancer is accompanied by a progressive upregulation of ATP6L, which closely parallels a spectrum of vascular abnormalities, including microvessel shrinkage, lumen narrowing, and pericyte dropout. Mechanistically, ATP6L overexpression appears to instigate pericyte dysfunction through an acidification-driven PDGFB/PDGFRβ signaling axis: ATP6L overexpression promotes an acidic microenvironment that suppresses PDGFB secretion, leading to reduced PDGFRβ expression on pericytes and consequently impairing their recruitment and survival. Conversely, ATP6L depletion reverses this deleterious cascade, restoring pericyte proliferation, migration, and survival. This work seeks to identify ATP6L as a novel modulator of the tumor vasculature, revealing a direct link between tumor acidification and vascular dysfunction. Together, these findings identify a novel link between tumor microenvironmental acidification and vascular abnormalities, suggesting ATP6L as a potential therapeutic target to normalize tumor vasculature and improve treatment efficacy.

2. Materials and Methods

2.1. Patient tissue specimens and clinical data

A total of 179 cases of surgically resected, pathologically confirmed colorectal cancer (CRC) specimens, along with corresponding clinicopathological data, were retrospectively collected from the Department of Pathology at Tianjin Medical University Cancer Institute and Hospital between July 2014 and February 2015. Additionally, 29 cases of matched normal colorectal mucosa, adjacent adenoma, and primary adenocarcinoma tissue samples were included for serial analysis. The study was approved by the Institutional Review Board of Tianjin Medical University Cancer Institute and Hospital (Approval No. bc2020073), and informed consent was obtained from all participants. Patient demographics and clinical characteristics are summarized in Table 1.

2.2. Immunohistochemistry (IHC) and immunofluorescence (IF)

Formalin-fixed, paraffin-embedded tissue sections (4 μm thick) were processed for IHC and IF staining following standard protocols. The primary antibodies used included: anti-ATP6L (1:200, Abcam plc, America), anti-CD31 (1:100, Zsbio, Beijing, China), anti-α-SMA (1:200, Abcam plc, America), anti-PDGFB (1:150, Abcam plc, America), and anti-PDGFRβ (1:150, Abcam plc, America). Appropriate secondary antibodies and detection systems (DAB for IHC, Alexa Fluor-conjugated for IF) were applied. Hematoxylin was used for counterstaining.

ATP6L expression in tumor cells was evaluated independently by two experienced pathologists blinded to clinical outcomes. For each specimen, two representative fields at 200× magnification were selected from the tumor-normal mucosal interface where active angiogenesis was evident. ATP6L staining was considered positive when brown cytoplasmic granules were present. Staining intensity was graded on a scale of 0 to 2 (0: no staining; 1: weak; 2: strong). The percentage of immunoreactive tumor cells was scored on a scale of 1 to 3 (1: < 30%; 2: 30–80%; 3: > 80%). A composite score for each field was calculated by multiplying the intensity score by the percentage score. The final ATP6L expression score for each case was the average of the two field scores. Tumors were then classified as having low expression (average score 1–3) or high expression (average score 4–6). Please refer to the previously published literature for specific evaluation details (*18*).

For each IHC/IF-stained section, five representative fields of view (200x magnification) in the tumor invasive front were captured to quantify vascular parameters. All quantifications were performed using ImageJ software (National Institutes of Health, USA). Microvessel Density (MVD) was determined by counting CD31-positive endothelial cell clusters or single cells in each field (*19*). Any brown-stained endothelial cell or cell cluster clearly separated from adjacent vessels was counted as a single microvessel. The mean count per field was calculated. The lumen area (μm²) of each CD31+

Table 1. Clinicopathological characteristics of colorectal cancer patients

Characteristics	Number of patients (%)
Age	
< 50	35 (19.6)
≥ 50	144 (80.4)
Gender	
Male	102 (57.0)
Female	77 (43.0)
Size	
< 5cm	124 (69.3)
≥ 5cm	55 (30.7)
Differentiation	
Poor	48 (26.8)
High/ Moderate	131 (73.2)
Clinical stage	
I/II	93 (52.0)
III/IV	86 (48.0)
Lymph Node Metastasis	
Present	73 (40.8)
Absent	106 (59.2)
Distant Metastasis	
Present	34 (19.0)
Absent	145 (81.0)
ATP6L expression level	
Low	46 (25.7)
High	133 (74.3)

vessel was measured, and the equivalent diameter was calculated. Pericyte Coverage Index was defined as the percentage of CD31-positive vascular perimeter that was co-localized with α-SMA-positive staining. Automated co-localization analysis was performed on CD31/α-SMA double-IF images. The cutoff of 96.10% for dichotomizing pericyte coverage as "High" or "Low" was derived from the cohort mean.

2.3. Cell culture and transfection

Mouse colorectal cancer cell lines MC38 and CT26, and mouse vascular smooth muscle cells (MOVAS) were obtained from ATCC. All cell lines were authenticated *via* short tandem repeat profiling and tested regularly for mycoplasma contamination. CRC cells were cultured in DMEM supplemented with 10% FBS. MOVAS cells were cultured in smooth muscle cell growth medium. Stable cell lines of MC38 and CT26, including sh-control (Ctrl), sh-ATP6L (KD), empty Vector, and ATP6L overexpression (OE), were generated by lentiviral transduction and selected with puromycin (2 μg/mL) for two weeks.

2.4. *In vitro* co-culture and functional assays

An indirect co-culture system was employed. Stably transfected MC38 and CT26 cells were seeded in the lower chamber of 6-well plates. MOVAS cells were seeded on Transwell inserts (0.4 μm pore, Corning) placed in the same well, allowing the sharing of conditioned medium without direct cell-cell contact. After 48 hours of co-culture, MOVAS cells were collected for analysis.

MOVAS cell proliferation was assessed using the 5-ethynyl-2′-deoxyuridine (EdU) incorporation assay kit according to the manufacturer's protocol. The proliferation rate was expressed as the percentage of EdU-positive nuclei.

The migratory ability of MOVAS cells was evaluated using 24-well Transwell chambers (8 μm pore size). MOVAS cells (2×10^4) suspended in serum-free medium were seeded into the upper chamber, while the lower chamber contained conditioned medium from CRC cultures. After 24 hours, migrated cells on the lower membrane surface were fixed, stained with 0.1% crystal violet, and counted in five random fields (200x).

Apoptosis of MOVAS cells was detected using a TUNEL assay kit. The apoptotic index was calculated as the percentage of TUNEL-positive nuclei. Additionally, expression levels of cleaved caspase-3, Bax and Bcl-2 were analyzed by Western blot.

2.5. Extracellular acidification detection

Extracellular acidification was assessed using the P61 fluorescent pH probe. Cells were seeded in black, clear-bottom 96-well plates at 4×10^4 cells/well and cultured overnight. Before staining, cells were washed twice with dilution buffer and then incubated with P61 working solution in the dark at 37°C for 30 min. Fluorescence intensity was measured at excitation/emission wavelengths of 488/580 nm and normalized to the control group. Three replicate wells were analyzed per condition, and the mean values were plotted using GraphPad Prism.

2.6. Lactic acid treatment for MOVAS

Following cell attachment, the culture medium was removed, and the cell monolayer was rinsed once or twice with PBS. Subsequently, the cells were incubated with culture medium containing 5 mM lactic acid. After incubation for 24–48 hours at 37°C in a humidified atmosphere of 5% CO_2, MOVAS were collected, and total protein was extracted for Western blot analysis.

2.7. Animal Experiments

All animal procedures were approved by the Institutional Animal Care and Use Committee of Tianjin Medical University Cancer Institute and Hospital (Protocol No. AE-2022216). Six-week-old female nude mice were subcutaneously inoculated in the right dorsal flank with MC38-vector or MC38-ATP6L-overexpressing cells (5×10^6 cells in 100 μL PBS per mouse) to induce tumor development. When tumors reached an average volume of 200 mm^3, tumor-bearing mice were randomly divided into three groups (n=6 per group): (a) Vector control, (b) ATP6L-overexpressing (OE), and (c) ATP6L-OE treated with Baf A1. Baf A1 was dissolved in a vehicle consisting of 10% DMSO, 40% PEG300, 5% Tween-80, and 45% saline, prepared fresh before each injection and sonicated to clarity (final concentration 2.5 mg/mL). Mice in the Baf A1 treatment group received intratumoral injections of Baf A1 at 5 mg/kg body weight (40 μL per injection) three times per week, while mice in the Vector and OE groups received equal-volume vehicle injections on the same schedule. This locally administered dose was chosen based on the reported anti-tumor efficacy of systemically delivered Baf A1 at 0.1–1 mg/kg and precedent for intratumoral Baf A1 administration in xenograft models, with local delivery adjusted to maximize target engagement while reducing off-target effects. Four weeks after treatment initiation, tumor tissue samples from each group were collected and subjected to histological evaluation. Tumor volume was measured twice weekly and calculated using the formula: Volume = (Length × $Width^2$)/2.

2.8. Analysis of *in vivo* vascular function and architecture

To evaluate functional vessel density and vascular permeability, we intravenously administered DyLight 594-conjugated lectin, which binds to the endothelial

glycocalyx to label perfused vessels, and FITC-dextran, which extravasates through leaky vessels. Vascular permeability and perfusion were assessed one day before euthanasia. Mice were intravenously injected with 100 μL of 2 mg/mL FITC-dextran (70 kDa). After 30 minutes, mice were anesthetized, and a subset (n = 3 per group) received an intracardiac injection of 100 μL of DyLight 594-conjugated Lycopersicon esculentum lectin to label perfused vessels. Tumor vessels were imaged using a two-photon microscope. Vessel permeability was quantified as the ratio of FITC-dextran intensity in the perivascular area to that within the vessel lumen. Perfused vessel density was calculated from lectin-positive areas. For immunofluorescence analysis of tumor sections, the pericyte coverage index was determined as described above.

2.9. Statistical analysis

Statistical analyses were performed using SPSS 25.0 (IBM) and GraphPad Prism 9.0. The distribution of data was assessed for normality using the Shapiro-Wilk test; for comparisons between two groups, an unpaired two-tailed Student's t-test (for normally distributed data) or the Mann-Whitney U test (for non-normally distributed data) was used. For comparisons among multiple groups, one-way ANOVA followed by Tukey's post-hoc test or the Kruskal-Wallis test with Dunn's post-hoc test was applied, as appropriate. Correlation analyses were performed using Pearson's or Spearman's correlation coefficient. Categorical data were analyzed using the Chi-square test. Data are presented as mean ± standard deviation (SD). A p-value < 0.05 was considered statistically significant. The "n" for each experiment indicates the number of biological replicates, as detailed in the figure legends.

3. Results

3.1. Vascular instability increases during normal mucosa-adenoma-adenocarcinoma sequence in CRC

To investigate the evolution of vascular morphology during CRC development, we performed double immunofluorescence staining for CD31 (endothelial marker) and α-SMA (pericyte/smooth muscle cell marker) on 29 matched tissue sets containing normal mucosa, adenoma and adenocarcinoma. Normal mucosa exhibited regular microvessels with a circular or oval shape and uniform thin walls, in adenoma, vascular morphology remained relatively regular, in contrast, adenocarcinoma tissue displayed vessels with impaired integrity, irregular shapes, variable diameters, and uneven wall thickness (Figure 1A). Quantitative analysis of the 29 paired samples showed a significant progressive decrease in pericyte coverage from normal mucosa to adenoma to adenocarcinoma (Normal mucosa: 96.8% ± 2.1%; Adenoma: 92.5% ± 4.3%; Adenocarcinoma: 76.4% ± 9.8%) (Figure 1B). While the mean microvessel density (MVD), lumen diameter, and lumen area did not differ significantly among the three groups, the distribution of these parameters was markedly more heterogeneous in adenoma and adenocarcinoma tissues (Supplementary Figure S1A-C, *https://www.biosciencetrends.com/action/getSupplementalData.php?ID=317*). Across the entire cohort of 179 CRC cases, poorly differentiated tumors showed significantly lower pericyte coverage than well/moderately-differentiated tumors (Figure 1D).

These observations indicate that vascular instability, characterized by immature morphology and reduced pericyte attachment, progressively increases during CRC development and correlates with poorer histological differentiation.

3.2. ATP6L expression negatively correlates with vascular stability and PDGFRβ signaling in human CRC tissues

Given the established role of ATP6L in promoting tumor malignancy, we next examined its relationship with vascular stability. In the matched tissue sequence, ATP6L expression, assessed by IHC score, progressively increased from normal mucosa to adenocarcinoma (Table 2). In the 179 CRC tissues, tumors with high ATP6L expression exhibited significantly larger microvascular luminal diameters and cross-sectional areas compared with their ATP6L-low counterparts (Figures 2B,2C), indicative of a dilated and aberrant vascular phenotype. Representative images of double CD31/α-SMA staining revealed scattered pericyte distribution and lower pericyte coverage in ATP6L-high tumors (Figure 2D). A significant negative correlation was confirmed between ATP6L expression and pericyte coverage index across the cohort (Figure 2E).

The interaction between PDGFB and PDGFRβ is a critical determinant of vascular stability. While PDGFB/PDGFRβ signaling is known to play a role in pericyte recruitment and vascular maturation, its precise contribution to tumor angiogenesis and vascular remodeling across different tumor contexts remains incompletely understood (*20,21*). IHC staining was then performed to examine the correlation between ATP6L expression and the protein levels of PDGFB and PDGFRβ in CRC specimens. Interestingly, CRC tissues with low ATP6L expression exhibited markedly elevated PDGFB levels alongside reduced stromal PDGFRβ expression. In contrast, tissues with high ATP6L expression showed significantly decreased PDGFB levels and increased stromal PDGFRβ levels (Figure 2F). This inverse relationship between ATP6L and PDGFRβ suggests a potential disruption in the crucial PDGFB/PDGFRβ signaling axis required for pericyte recruitment and maintenance.

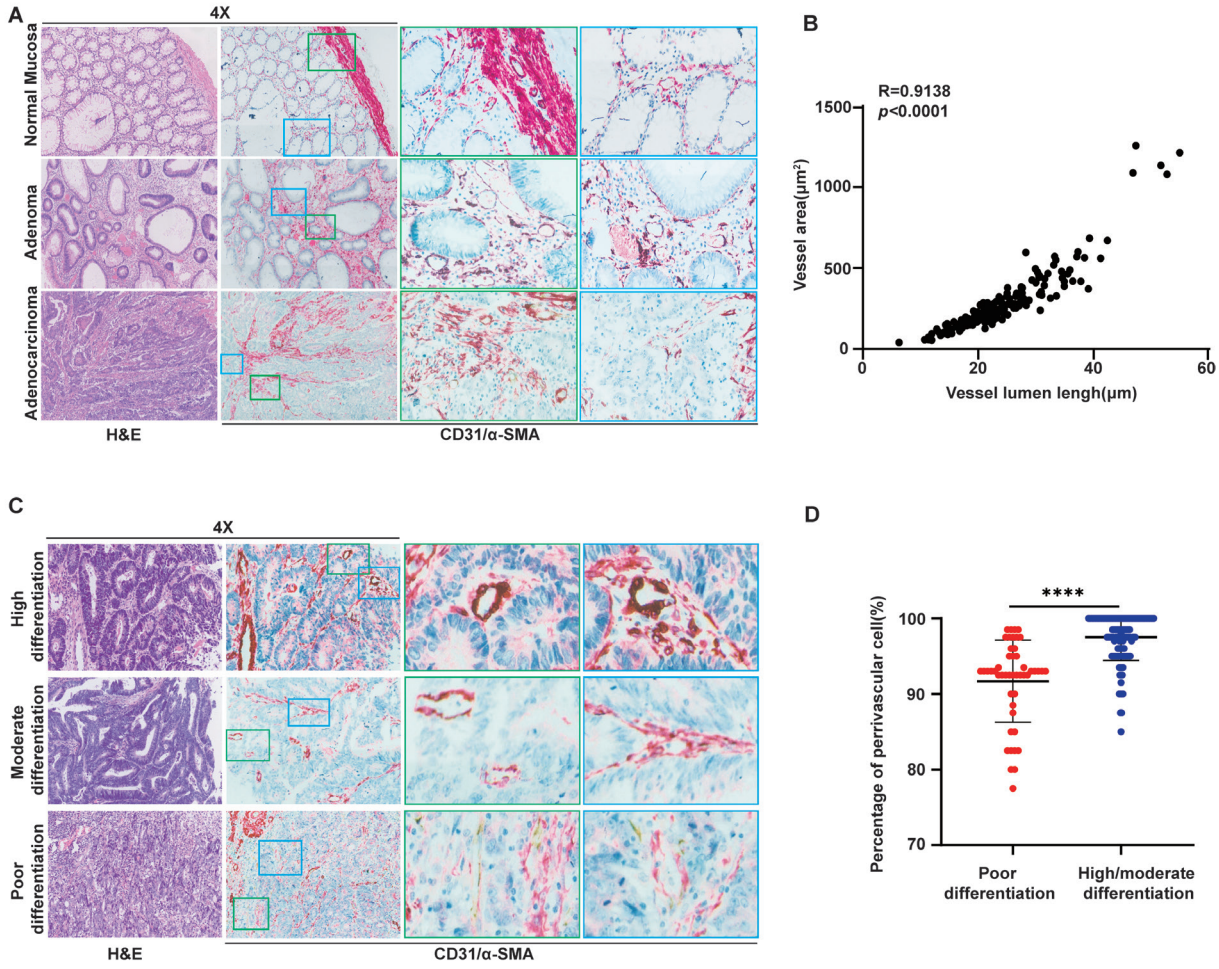

Figure 1. Vascular instability increases during colorectal cancer progression and correlates with tumor differentiation. (A). HE staining and representative immunofluorescence images of human colonic tissues stained for the endothelial cell marker CD31 (brown) and the pericyte marker α-SMA (red) in normal colonic mucosa, adenoma and adenocarcinoma. Insets 1 and 2 show higher-magnification images of the vessels (boxed areas). **(B).** Quantitative analysis of pericyte coverage in 29 matched normal mucosa-adenoma-adenocarcinoma tissue trios. Data are presented as mean ± SD. $P < 0.001$; one-way ANOVA with Tukey's post-hoc test. **(C).** HE staining and α-SMA/CD31 double staining to assess the relationship between differentiation grade and perivascular cell coverage in 179 cases. **(D).** Comparison of pericyte coverage between poorly differentiated (n = 48) and high/moderate differentiated (n = 131) tumors in the 179-case cohort. Data are presented as mean ± SD. ****, $p < 0.0001$.

Table 2. ATP6L expression during the colorectal normal mucosa-adenoma–adenocarcinoma sequence

	ATP6L expression *n* (%)			X^2	*p* value
	Total	Low expression	High expression		
Normal mucosa	29	27 (93.1)	2 (6.9)	39.518	$P < 0.001$
Adenoma	29	20 (67.0)	9 (33.0)		
Adenocarcinoma	29	4 (13.8)	25 (86.2)		
Total	87	51 (58.6)	36 (41.4)		

3.3. ATP6L overexpression in CRC cells inhibits pericyte function and disrupts PDGFB/PDGFRβ signaling *in vitro*

To establish causality, we generated stable MC38 and CT26 cell lines with ATP6L overexpression (OE) and corresponding Vector controls, respectively (Figure 3A). Using an indirect co-culture system (Figure 3B), we found that the conditioned medium from ATP6L-OE cells significantly increased extracellular H^+ concentration, confirming enhanced acidification (Figure 3C). Conditioned medium from ATP6L-OE cells not only potently inhibited the proliferation and migration of MOVAS, a pericyte model (Figures 3D,3E), but also promoted its apoptosis. This pro-apoptotic effect was supported by both molecular changes—increased Bax/Bcl-2 ratio and cleaved Caspase-3 (Figure 3F)—and a

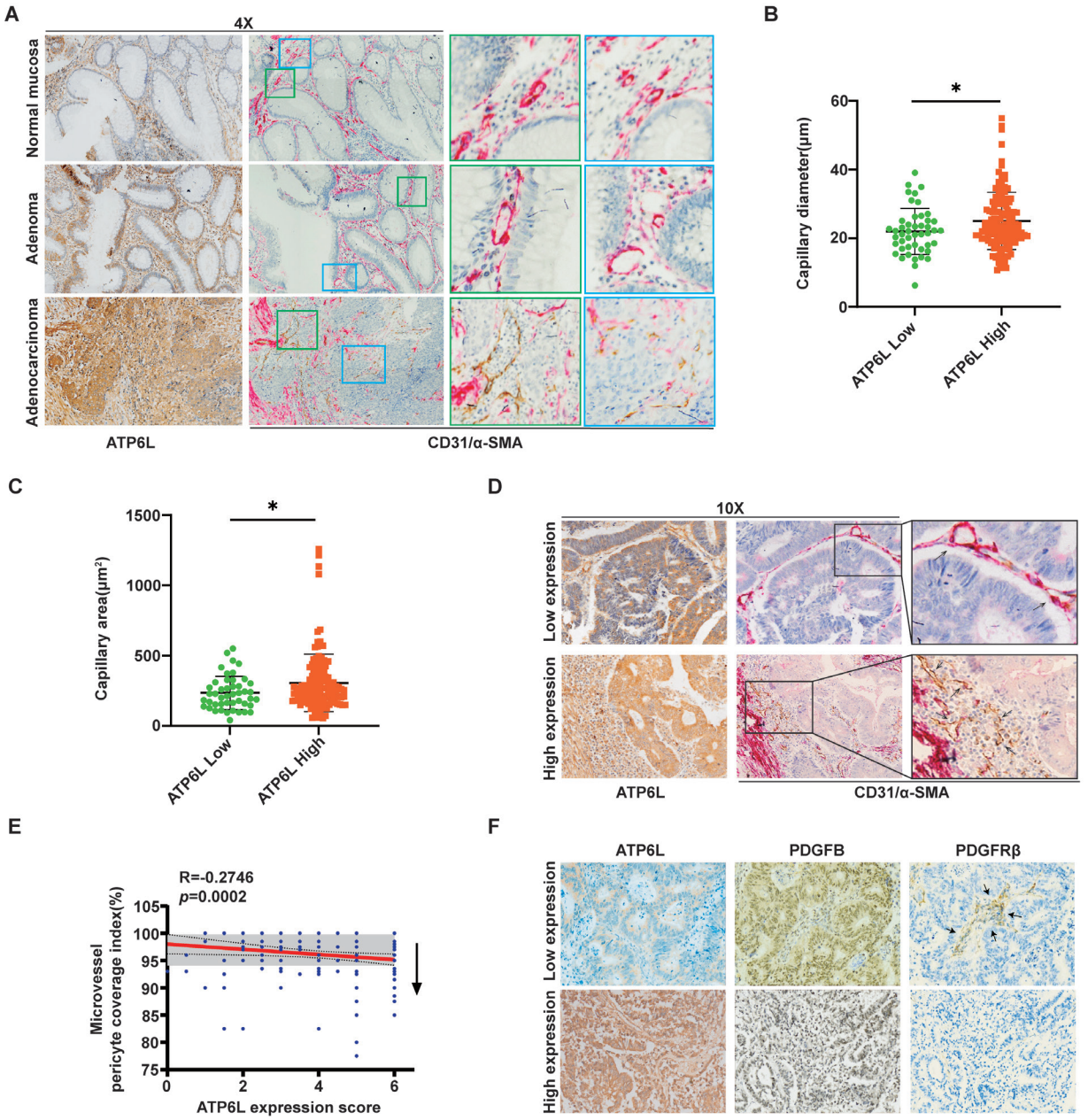

Figure 2. ATP6L expression is associated with vascular instability and PDGFRβ signaling dysregulation in human CRC. (A). Representative images of ATP6L immunohistochemistry and CD31/α-SMA double immunohistochemistry staining in normal mucosa and adenocarcinoma tissues, showing samples labeled as "normal mucosa," "adenoma," and "adenocarcinoma," respectively. **(B)**, **(C)**. Quantification of microvascular lumen diameter **(B)** and lumen area **(C)** in CRC tissues with ATP6L high expression *vs.* ATP6L low expression. **(D).** Representative images of CD31/α-SMA double immunofluorescence staining in colorectal cancer tissues with different ATP6L expression levels. **(E).** Correlation between ATP6L expression and pericyte coverage index (%) in 179 CRC tissues. Spearman's correlation analysis. **(F).** Representative immunohistochemical staining images showing ATP6L, PDGFB and PDGFRβ expression in serial sections of CRC tissues. *, $p < 0.05$.

2.8-fold increase in TUNEL-positive cells (Figure 3G).

Recapitulating the observations from CRC specimens, our mechanistic investigations revealed a significant reduction in PDGFRβ concentration in the co-culture medium of ATP6L-OE cells (Figure 3H). It has been reported that lactate can be taken up and utilized by pericytes for energy generation and various biogenic processes, which are critical for normal pericyte function (*22,23*). Given that ATP6L-OE cells markedly increased extracellular H^+ concentration, we hypothesized that ATP6L overexpression in CRC cells creates an acidic extracellular milieu that in turn suppresses PDGFB secretion. To test this hypothesis, we sought to block the acidic environment induced by ATP6L-OE using Bafilomycin A1 (Baf A1), a specific and reversible inhibitor of V-ATPase that prevents intracellular acidification (*24*). Concurrently, ELISA results demonstrated that the PDGFB protein concentration in the co-culture supernatant was significantly reduced in MOVAS cells co-cultured with MC38/

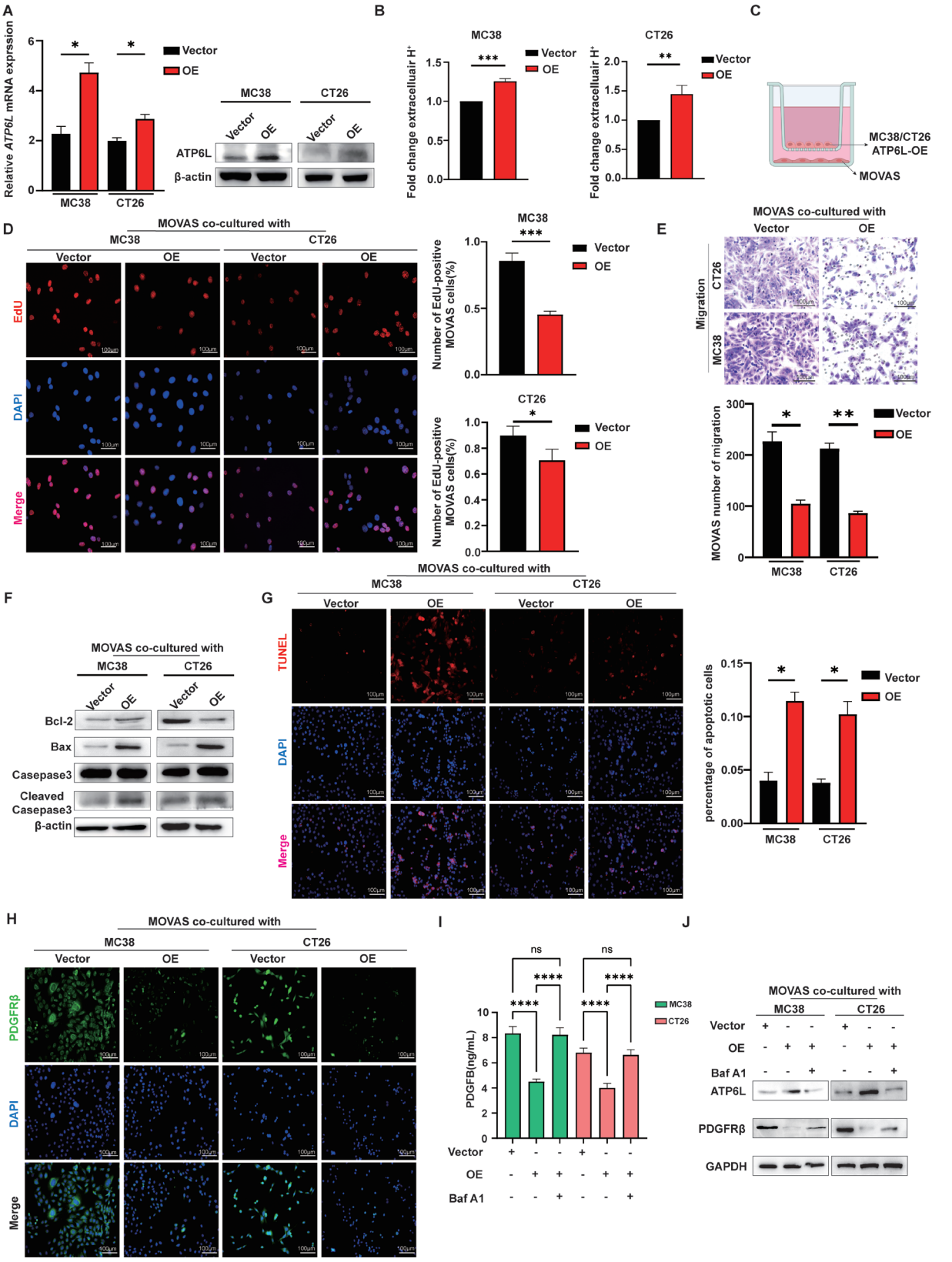

Figure 3. ATP6L overexpression in CRC cells impairs pericyte function and dysregulates PDGFB/PDGFRβ signaling *in vitro*. **(A).** Validation of ATP6L overexpression in MC38 and CT26 cell lines at the mRNA and protein levels. **(B).** Extracellular acidification rate detected by the P61 pH-sensitive fluorescent probe in conditioned medium from Vector and ATP6L-overexpressing (ATP6L-OE) CRC cells. **(C).** Co-culture of MOVAS cells with MC38/CT26. **(D).** Proliferation of mouse vascular smooth muscle cells (MOVAS) after 24-hour co-culture with CRC cells, assessed by EdU incorporation assay—representative images and quantification for MC38 and CT26 co-cultures. **(E).** Migration of MOVAS cells assessed by Transwell assay after co-culture. Representative images and quantification. F&G. Apoptosis of MOVAS cells. Western blot analysis of apoptosis-related proteins **(F).** and representative TUNEL staining images, quantification of TUNEL-positive cells **(G)**. **(H).** Expression of PDGFRβ in MOVAS cells after co-culture, detected by immunofluorescence. **(I).** Quantification of PDGFB concentration in co-culture medium by ELISA. **(J).** Western blot analysis of PDGFRβ expression in different co-culture systems. Data are presented as mean ± SD from at least three independent experiments. Scale bars, 100 μm.*, $p < 0.05$; **, $p < 0.01$; ***, $p < 0.001$; ****, $p < 0.0001$; ns, not significant. Unpaired two-tailed *t*-test.

CT26 ATP6L-OE cells, relative to the Vector control group. Correspondingly, PDGFRβ protein expression in MOVAS cells was markedly downregulated in both ATP6L-OE co-culture groups. Importantly, pre-treatment of ATP6L-OE cells with Baf A1 partially restored both the supernatant PDGFB concentration and the PDGFRβ expression level in MOVAS cells (Figures 3I,3J).

To further explore the mechanistic link between ATP6L and the PDGFB/PDGFRβ axis in the context of CRC pericyte function and vascular stability, we generated ATP6L-knockdown (ATP6L-KD) MC38 and CT26 cell lines (Figure 4A) and carried out parallel experiments. Compared with the control group, MOVAS cells co-cultured with ATP6L-KD MC38/CT26 cells (Figure 4B) exhibited enhanced proliferation and migration and reduced apoptosis (Figures 4C–F). We found conditioned medium from ATP6L-KD cells significantly decreased extracellular H^+ concentration, indicating attenuated acidification (Figure 4G). ELISA showed that co-culture with ATP6L-KD cells elvated supernatant PDGFB secretion (Figure 4H), while Western blot analysis revealed that PDGFRβ protein levels were inversely correlated with ATP6L expression. To assess the functional contribution of ATP6L's proton-pumping activity, we treated ATP6L-KD cells with lactate, which partially reversed the reduction in PDGFB secretion. Consistently, this exogenous H^+ supplementation also abrogated the ATP6L-KD-induced alterations in PDGFRβ expression (Figure 4I). These pH fluctuations, in turn, may serve as a regulatory mechanism for the PDGFB/PDGFRβ axis.

Collectively, these *in vitro* data support a model in which ATP6L regulates the PDGFB/PDGFRβ signaling axis by modulating extracellular H+ levels, thereby influencing pericyte function and vascular stability.

3.4. ATP6L overexpression compromises vascular stability and perfusion *in vivo*

We sought to verify these *in vitro* findings in an *in vivo* model with MC-38 cells. The mouse tumor xenograft model was established by subcutaneously implanting either ATP6L-OE or Vector MC38 cells into the groins of each nude mouse. ATP6L-OE tumors exhibited significantly larger volumes than Vector controls, and intratumoral Baf A1 administration effectively inhibited their *in vivo* growth (Figure 5A). Upon tumor dissection, the subcutaneous tumorigenic active area in the ATP6L-OE group was found to be significantly larger than that in the Vector group. Notably, intratumoral injection of Baf A1 effectively promoted apoptosis within the tumors (Figure 5B). Meanwhile, lectin perfusion and FITC-dextran extravasation assays revealed that ATP6L-OE tumors exhibited a 30% reduction in functional vessel density and a 2.1-fold increase in permeability. Notably, these vascular abnormalities were partially reversed upon intratumoral administration of Baf A1 (Figure 5C).

To address pericyte heterogeneity and avoid marker-specific bias, we assessed pericyte coverage using three markers—α-SMA, NG2 and PDGFRβ—in combination with CD31. All three markers exhibited significantly reduced co-localization with CD31 in ATP6L-OE tumors, confirming global pericyte dysfunction. Notably, this vascular defect was partially rescued by intratumoral administration of Baf A1, which effectively reversed the vascular dysfunction induced by ATP6L overexpression (Figure 5D). Collectively, these findings confirm that ATP6L overexpression in tumor cells is sufficient to drive vascular instability and dysfunction *in vivo.*

4. Discussion

The role of ATP6L in promoting tumor malignancy has been confirmed in studies of other cancer types, including hepatocellular carcinoma (*14*), breast cancer (*15*), and pancreatic cancer (*16*). Our group has previously demonstrated that ATP6L is highly expressed in poorly differentiated CRC and promotes tumor cell mesenchymal-epithelial transition (*17*). However, the relationship between ATP6L and angiogenesis or vascular stability remains poorly understood. Here, we identify a novel role for ATP6L, a key subunit of the V-ATPase proton pump, in driving vascular instability in CRC. Specifically, we found that high ATP6L expression in CRC cells is both clinically correlated with and functionally sufficient to reduce pericyte coverage and disrupt normal vascular architecture, culminating in a dysfunctional and hyperpermeable tumor vasculature.

Our analysis of the adenoma–adenocarcinoma sequence corroborates the notion of progressive vascular maladaptation accompanying colorectal tumorigenesis (*1,25,26*). Specifically, we observed a marked reduction in pericyte coverage along the normal mucosa–adenoma–adenocarcinoma continuum, reflecting progressive vessel immaturity. This vascular instability was further exacerbated in poorly differentiated tumors, implying a close relationship between aggressive cancer phenotypes and a compromised stromal microenvironment (*1,2,27*). Importantly, the selective association of high ATP6L expression with enlarged, tortuous vessels and diminished pericyte coverage in human CRC specimens implicates ATP6L as a key mediator that bridges tumor-intrinsic acidification and perivascular dysfunction.

Mechanistically, our functional data support a model linking tumor cell acidification to pericyte dysfunction and vascular instability *via* the PDGFB/PDGFRβ signaling axis. PDGFB/PDGFRβ signaling is a critical determinant of vascular stability (28,29), yet in tumors, pericytes are typically sparse and form loose associations with endothelial cells (*30,31*). This may partly arise from tumor-derived PDGFB, which disrupts the physiological PDGFB/PDGFRβ gradient (*32*). Although this signaling axis has been implicated in pericyte

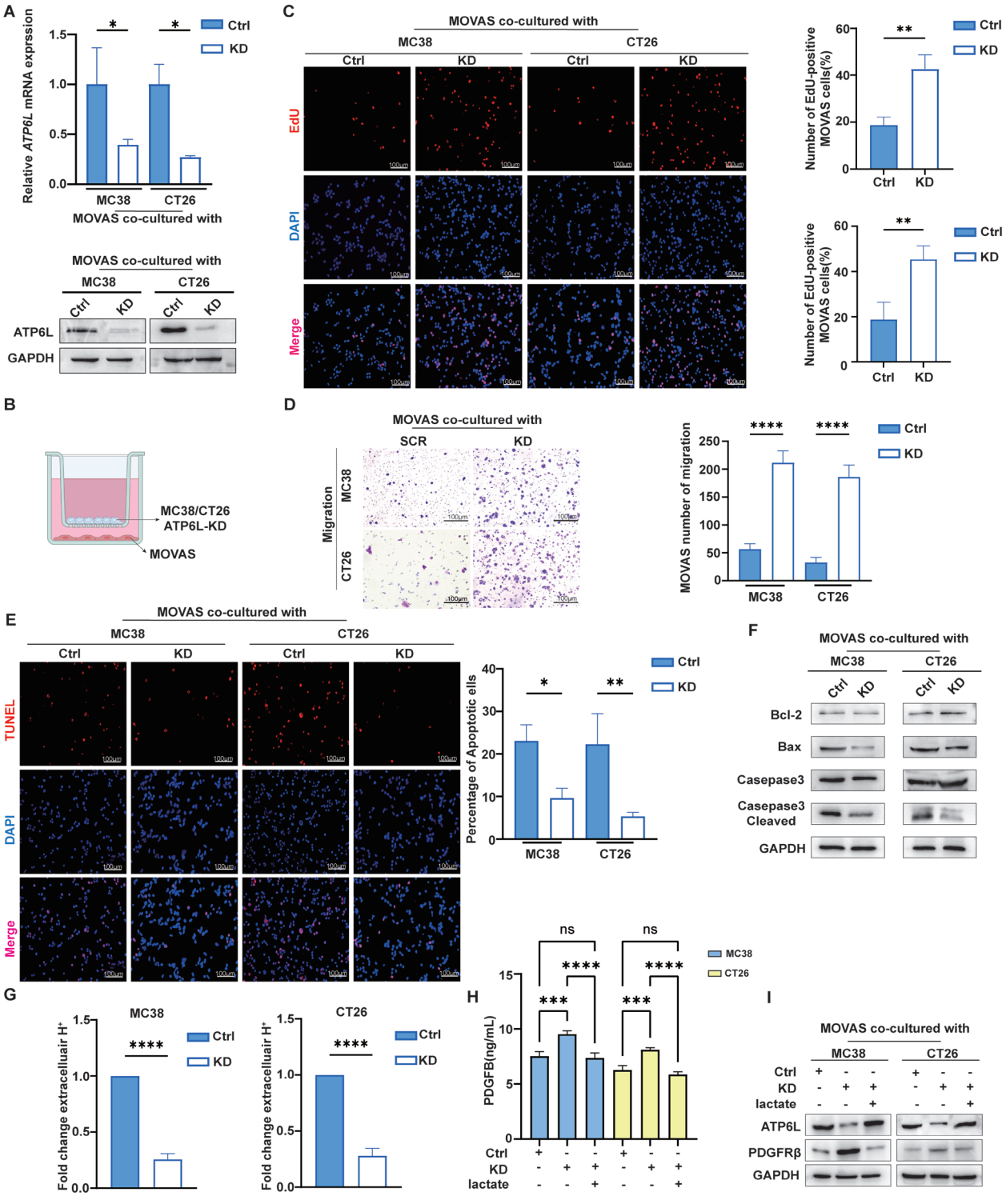

Figure 4. ATP6L knockdown in CRC cells enhances pericyte function and activates PDGFB/PDGFRβ signaling *in vitro*. (A). Validation of ATP6L knockdown in MC38 and CT26 cell lines at the mRNA and protein levels. **(B).** Co-culture of MOVAS cells with MC38/CT26. **(C).** Proliferation of mouse vascular smooth muscle cells (MOVAS) after 24-hour co-culture with CRC cells, assessed by EdU incorporation assay—representative images and quantification for MC38 and CT26 co-cultures. **(D).** Migration of MOVAS cells assessed by Transwell assay after co-culture. Representative images and quantification. E&F. Apoptosis of MOVAS cells. Western blot analysis of apoptosis-related proteins **(E)** and representative TUNEL staining images, quantification of TUNEL-positive cells **(F)**. **(G).** Extracellular acidification rate detected by the P61 pH-sensitive fluorescent probe in conditioned medium from control (Ctrl) and ATP6L-knockdown (ATP6L-KD) CRC cells. **(H).** Quantification of PDGFB concentration in co-culture medium by ELISA. **(I).** Western blot analysis of PDGFRβ expression in different co-culture systems. Data are presented as mean ± SD from at least three independent experiments. Scale bars, 100 μm.*, $p < 0.05$; **, $p < 0.01$; ***, $p < 0.001$; ****, $p < 0.0001$; ns, not significant. Unpaired two-tailed *t*-test.

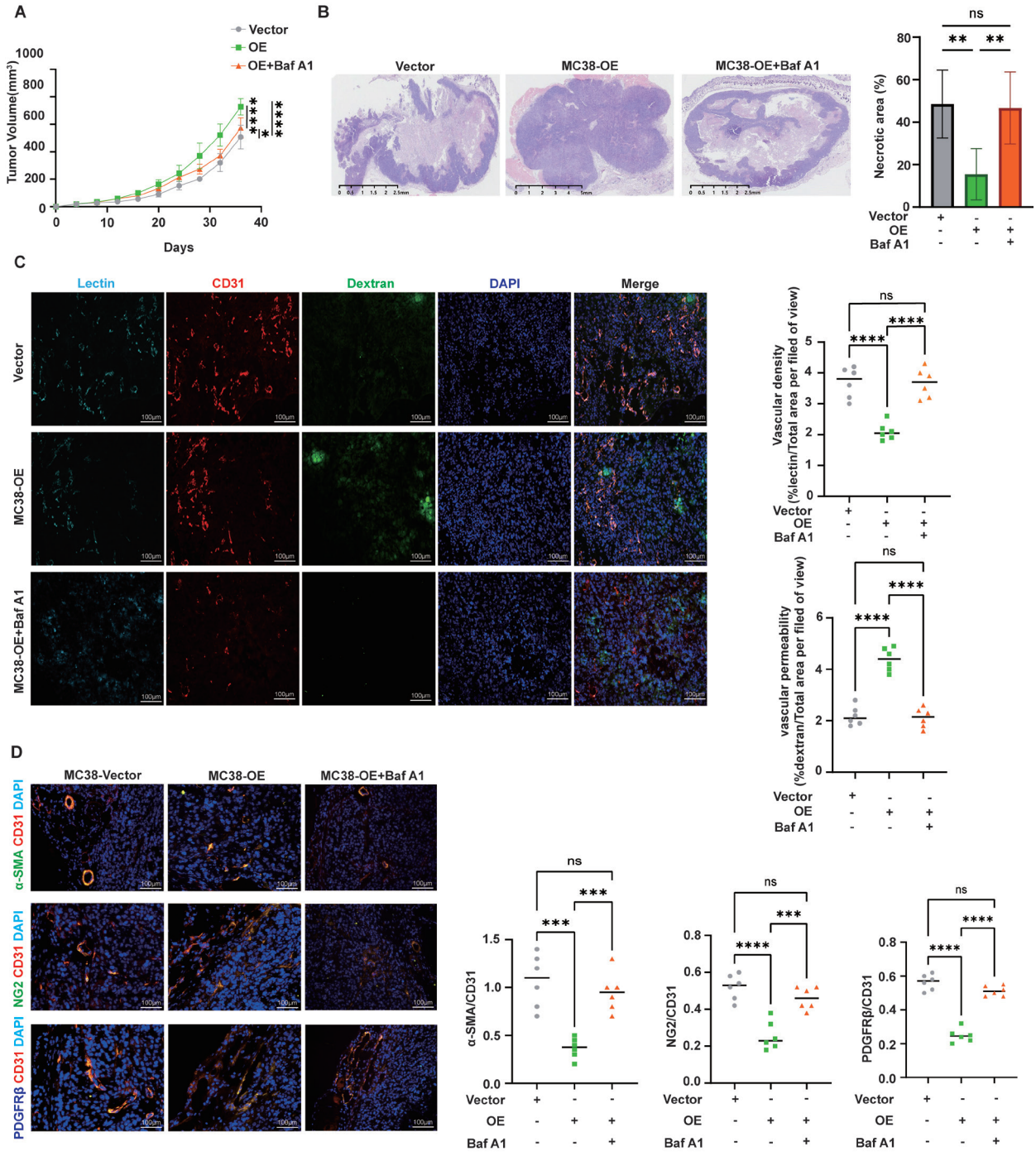

Figure 5. ATP6L overexpression compromises vascular stability and perfusion *in vivo*. (A). *In vivo* tumor growth curves. **(B).** Tumor necrosis under different conditions, H&E staining and quantification. **(C).** Analysis of tumor vasculature in MC38 xenograft models. Representative merged images of perfused vessels (Lectin, blue), endothelial marker CD31 (red), and permeable vasculature (FITC-dextran, green). Quantification of perfused vessel density and vascular permeability index. **(D).** Assessment of pericyte coverage in tumor xenografts. Representative immunofluorescence images showing co-localization of the endothelial marker CD31 (red) with pericyte markers α-SMA, NG2 and PDGFRβ (green). Scale bars, 100μm. Quantification of pericyte coverage for each marker.*, $p < 0.05$;**, $p < 0.01$;***, $p < 0.001$; ****, $p < 0.0001$; ns, not significant.

recruitment and vascular maturation, its precise role in tumor angiogenesis and vascular remodeling remains incompletely understood and appears to be context-dependent (*1,30,33*).

We find that ATP6L overexpression in CRC cells acidifies the extracellular space and suppresses PDGFB secretion. This reduction in PDGFB, acting paracrinally, downregulates PDGFRβ expression on pericytes, thereby disrupting a signaling cascade critical for their recruitment and survival. The resultant pericyte dysfunction—manifested as reduced proliferation, impaired migration, and heightened apoptosis—is consistent with our phenotypic observations. Moreover, ATP6L expression levels directly correlate with changes

in intracellular pH, which in turn modulate PDGFB/PDGFRβ signaling. *In vivo*, ATP6L-overexpressing tumors exhibit a dysfunctional vasculature with poor perfusion, elevated permeability, and sparse pericyte coverage. Together, these findings support a model in which ATP6L regulates the PDGFB/PDGFRβ axis *via* extracellular H^+, thereby regulating pericyte function and vascular stability. A schematic representation of the proposed ATP6L–extracellular acidification–PDGFB/PDGFRβ–pericyte axis is shown in Figure 6.

In our model, ATP6L overexpression creates an acidic microenvironment that suppresses PDGFB secretion, thereby reducing PDGFRβ expression on pericytes and impairing vascular stability. Of note, a previous study by Hosaka *et al*. has shown that in tumors with high PDGFB expression, sustained exposure to elevated PDGFB levels can also cause pericyte loss through PDGFRβ internalization and degradation (*34*). Thus, insufficient PDGFRβ signaling, arising from either decreased ligand availability or receptor downregulation, underlies pericyte dysfunction and vascular instability in both contexts. These observations underscore that the integrity of PDGFRβ signaling is essential for maintaining vascular stability, while the upstream regulatory mechanisms may vary by tumor type and microenvironmental context.

Translationally, our findings suggest that ATP6L could serve as both a biomarker for metastasis-prone unstable vasculature and a therapeutic target for vascular normalization. Targeting ATP6L may reverse PDGFB/PDGFRβ dysregulation, stabilize tumor vessels, and improve drug delivery, potentially overcoming the hypoxia-driven invasiveness associated with current anti-angiogenic therapies. However, limitations include the observational nature of human tissue correlations, the preliminary mechanistic data, and the use of murine cell models—all of which warrant cautious interpretation.

In conclusion, we demonstrate that ATP6L is a critical driver of vascular instability in colorectal cancer. By promoting a tumor-acidified microenvironment that disrupts the PDGFB/PDGFRβ signaling axis, ATP6L undermines pericyte function, leading to a leaky, immature vasculature. Targeting this axis may offer a novel strategy to normalize the tumor vasculature and improve therapeutic outcomes.

Funding: This work was supported by grants from the National Natural Science Foundation of China

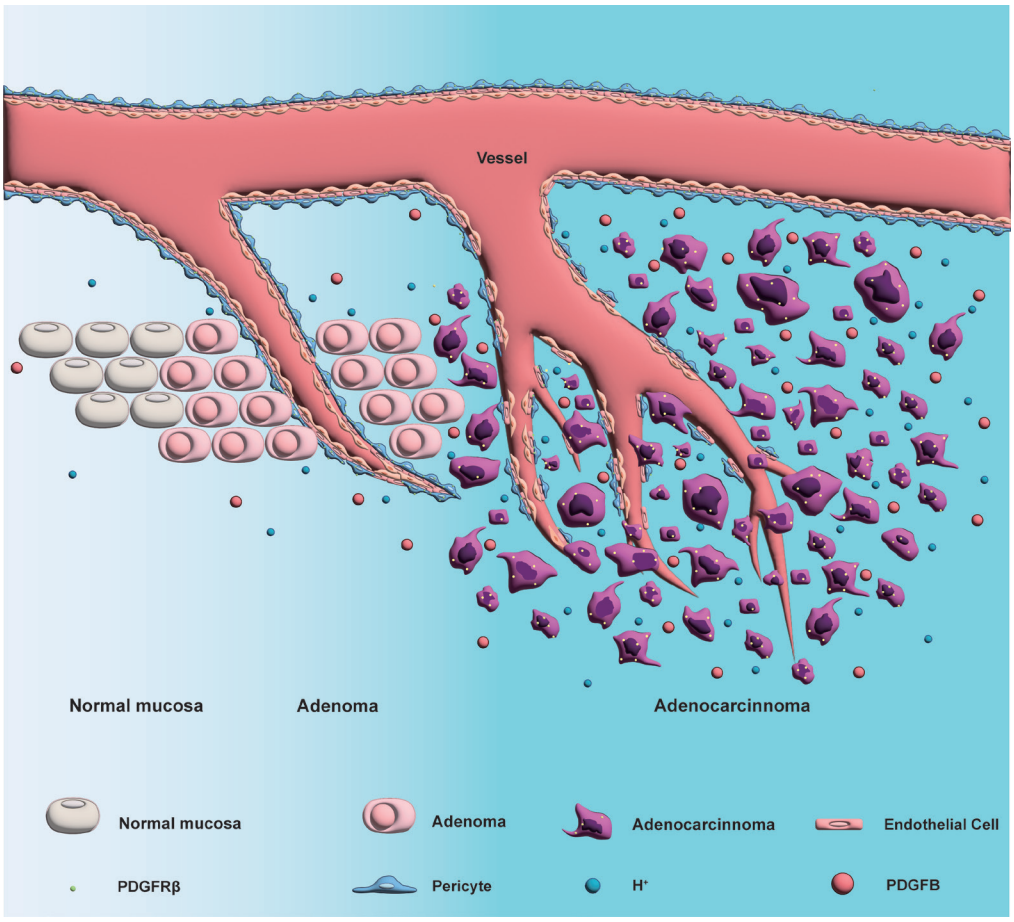

Figure 6. Proposed model of ATP6L-mediated vascular destabilization through extracellular acidification and dysregulation of the PDGFB/PDGFRβ axis in colorectal cancer.

(82472991), Natural Science Foundation of Tianjin (23JCYBJC00600), and Tianjin Key Medical Discipline Construction Project (TJYXZDXK-3-016C).

Conflict of Interest: The authors have no conflicts of interest to disclose.

Ethics approval: The human component of this study involving patient participation was approved by the Ethics Committee of Tianjin Medical University Cancer Institute and Hospital (Approval No. bc2020073) in accordance with the Declaration of Helsinki. The animal experiments were approved by the same ethics committee (Approval No. AE-2022216) in accordance with NIH Guidelines for Animal Research.

References

1. Guelfi S, Hodivala-Dilke K, Bergers G. Targeting the tumour vasculature: from vessel destruction to promotion. Nat Rev Cancer. 2024; 24:655-675.
2. Martin JD, Seano G, Jain RK. Normalizing Function of Tumor Vessels: Progress, Opportunities, and Challenges. Annu Rev Physiol. 2019; 81:505-534.
3. Magnussen AL, Mills IG. Vascular normalisation as the stepping stone into tumour microenvironment transformation. Br J Cancer. 2021; 125:324-336.
4. Jain RK. Normalization of tumor vasculature: an emerging concept in antiangiogenic therapy. Science. 2005; 307:58-62.
5. Jordan AM, Drake RJG, Hodivala-Dilke KM. Angiocrine and pericrine signaling: how endothelial cells and pericytes drive cancer progression and therapy resistance. Physiol Rev. 2026; 106:87-119.
6. Tian L, Goldstein A, Wang H, *et al*. Mutual regulation of tumour vessel normalization and immunostimulatory reprogramming. Nature. 2017; 544:250-254.
7. Zhu J, Yang W, Ma J, He H, Liu Z, Zhu X, He X, He J, Chen Z, Jin X, Wang X, He K, Wei W, Hu J. Pericyte signaling *via* soluble guanylate cyclase shapes the vascular niche and microenvironment of tumors. EMBO J. 2024; 43:1519-1544.
8. Gomez D, Owens GK. Smooth muscle cell phenotypic switching in atherosclerosis. Cardiovasc Res. 2012; 95:156-164.
9. Pan X, Li X, Dong L, *et al*. Tumour vasculature at single-cell resolution. Nature. 2024; 632:429-436.
10. Swietach P, Boedtkjer E, Pedersen SF. How protons pave the way to aggressive cancers. Nat Rev Cancer. 2023; 23:825-841.
11. Corbet C, Feron O. Tumour acidosis: from the passenger to the driver's seat. Nat Rev Cancer. 2017; 17:577-593.
12. Forgac M. Vacuolar ATPases: rotary proton pumps in physiology and pathophysiology. Nat Rev Mol Cell Biol. 2007; 8:917-929.
13. Cotter K, Capecci J, Sennoune S, Huss M, Maier M, Martinez-Zaguilan R, Forgac M. Activity of plasma membrane V-ATPases is critical for the invasion of MDA-MB231 breast cancer cells. J Biol Chem. 2015; 290:3680-3692.
14. Zeng S, Chen J, Ren Y, *et al*. Multiscale imaging on proton pump-driven acidity for assessing tumor progression and metastasis. Nat Commun. 2026; 17:1785.
15. You H, Jin J, Shu H, Yu B, Milito AD, Lozupone F, Deng Y, Tang N, Yao G, Fais S, Gu J, Qin W. Small interfering RNA targeting the subunit ATP6L of proton pump V-ATPase overcomes chemoresistance of breast cancer cells. Cancer Lett. 2009; 280:110-119.
16. Stransky L, Cotter K, Forgac M. The Function of V-ATPases in Cancer. Physiol Rev. 2016; 96:1071-1091.
17. Wang J, Chen D, Song W, Liu Z, Ma W, Li X, Zhang C, Wang X, Wang Y, Yang Y, Cao W, Qi L. ATP6L promotes metastasis of colorectal cancer by inducing epithelial-mesenchymal transition. Cancer Sci. 2020; 111:477-488.
18. Tian X, Xia Y, Gong W, Zhu K, Yang Y, Han Z, Liu Y, Li J, Li X, He Y, Gao M, Chen L, Guo H, Zhao Q. PLK4 as a Key Regulator of Neuroblastoma Differentiation and a Promising Therapeutic Target. Int J Biol Sci. 2025; 21:4979-4996.
19. Qin Y, Zhao W. The Modeling Analysis and Effect of CHI3L1 and CD31-Marked Microvessel Density in the Occurrence and Development of Cervical Squamous Cell Carcinoma. Comput Math Methods Med. 2022; 2022:3516335.
20. Guo Z, Cao Y. Mechanisms of Pericyte-Mediated Cancer Metastasis. Adv Sci (Weinh). 2026; 13:e00031.
21. Lee SJ, Kim S, Jo DH, Cho CS, Kim SR, Kang D, Chae J, Yoo DK, Ha S, Chung J, Kim JH. Specific ablation of PDGFRβ-overexpressing pericytes with antibody-drug conjugate potently inhibits pathologic ocular neovascularization in mouse models. Commun Med (Lond). 2021; 1:58.
22. Lee HW, Xu Y, Zhu X, Jang C, Choi W, Bae H, Wang W, He L, Jin SW, Arany Z, Simons M. Endothelium-derived lactate is required for pericyte function and blood-brain barrier maintenance. EMBO J. 2022; 41:e109890.
23. Zou MZ, Liu WL, Chen HS, Bai XF, Gao F, Ye JJ, Cheng H, Zhang XZ. Advances in nanomaterials for treatment of hypoxic tumor. Natl Sci Rev. 2021; 8:nwaa160.
24. Wang R, Wang J, Hassan A, Lee CH, Xie XS, Li X. Molecular basis of V-ATPase inhibition by bafilomycin A1. Nat Commun. 2021; 12:1782.
25. Liu Z, Sun B, Qi L, Li Y, Zhao X, Zhang D, Zhang Y. Dickkopf-1 expression is down-regulated during the colorectal adenoma-carcinoma sequence and correlates with reduced microvessel density and VEGF expression. Histopathology. 2015; 67:158-166.
26. Staton CA, Chetwood AS, Cameron IC, Cross SS, Brown NJ, Reed MW. The angiogenic switch occurs at the adenoma stage of the adenoma carcinoma sequence in colorectal cancer. Gut. 2007; 56:1426-1432.
27. Suvac A, Ashton J, Bristow RG. Tumour hypoxia in driving genomic instability and tumour evolution. Nat Rev Cancer. 2025; 25:167-188.
28. Abramsson A, Lindblom P, Betsholtz C. Endothelial and nonendothelial sources of PDGF-B regulate pericyte recruitment and influence vascular pattern formation in tumors. J Clin Invest. 2003; 112:1142-1151.
29. Lindahl P, Johansson BR, Levéen P, Betsholtz C. Pericyte loss and microaneurysm formation in PDGF-B-deficient mice. Science. 1997; 277:242-245.
30. Sun R, Kong X, Qiu X, Huang C, Wong PP. The Emerging Roles of Pericytes in Modulating Tumor Microenvironment. Front Cell Dev Biol. 2021; 9:676342.
31. Kasurinen JH, Hagström J, Kaprio T, Jalkanen S, Salmi M, Böckelman C, Haglund C. Prognostic Values of

Tissue and Serum Angiogenic Growth Factors Depend on the Phenotypic Subtypes of Colorectal Cancer. Cancers (Basel). 2023; 15.
32. Zhang Y, Cedervall J, Hamidi A, *et al*. Platelet-Specific PDGFB Ablation Impairs Tumor Vessel Integrity and Promotes Metastasis. Cancer Res. 2020; 80:3345-3358.
33. Huinen ZR, Huijbers EJM, van Beijnum JR, Nowak-Sliwinska P, Griffioen AW. Anti-angiogenic agents—overcoming tumour endothelial cell anergy and improving immunotherapy outcomes. Nat Rev Clin Oncol. 2021; 18:527-540.
34. Hosaka K, Yang Y, Seki T, *et al*. Tumour PDGF-BB expression levels determine dual effects of anti-PDGF drugs on vascular remodelling and metastasis. Nat Commun. 2013; 4:2129.

Received August 4, 2026; Revised August 25, 2026; Accepted August 27, 2026.

[§]These authors contributed equally to this work.
**Address correspondence to:*
Xiangdong Tian and Lisha Qi, Tianjin Medical University Cancer Institute and Hospital, West HuanHu Road, Ti Yuan Bei, Hexi District, Tianjin 300060, China.
E-mail: xiangdongtian@tmu.edu.cn; lqi01@tmu.edu.cn

Released online in J-STAGE as advance publication August 28, 2026.